STUDY OF SUPPORT INTERFERENCE EFFECTS AT S1MA WIND TUNNEL WITHIN THE "SAO" PROJECT

Aurélia Cartieri, S. Mouton, G. Boyet
ONERA

Keywords: *aerodynamics, wind tunnel, support interference*

Abstract

In this paper we try to introduce CFD to an unconventional place: the wind tunnel. The aim of this paper is to study the aerodynamic interference effects of two different stings supporting an aircraft model during wind tunnel tests. The flow field and forces distortion caused by the stings were deduced by comparing simulations with and without support. Comparison against experimental measurements thanks to dummy sting tests is provided for validation purpose.

1 Introduction

During wind tunnel tests the aircraft model is maintained in the test section thanks to a support system. This support is shaped to be as small and as discrete as possible, under the constraint that it should sustain forces generated over a wide range of flow conditions and enclose all cables and tubes necessary to supply energy and collect measurements from the embarked sensors.

Several recent ([1][3]) or older ([6]) initiatives aimed at determining whether advanced numerical simulations could help in understanding and predicting the support interference effect. This paper summarizes such an attempt carried out at ONERA on a transonic transport aircraft.

2 Description of experimental tests and numerical simulations

2.1 Model and supports

The aircraft model selected for this study was a full aircraft comprising the fuselage, the wing with four nacelles (non-powered), the vertical and horizontal tail planes (VTP and HTP). The wing shape is representative of state of the art aerodynamic design for this kind of civil aircraft.

The wind tunnel supports under study in this paper are:

- a straight sting made of cylindrical and conical pieces and penetrating the aircraft fuselage from behind, near the horizontal tail plane;
- a Z-sting, mainly composed of a conical sting supporting a blade which itself penetrates the rear fuselage of the model from below.

Those two supports and the model are presented in Fig. 1.

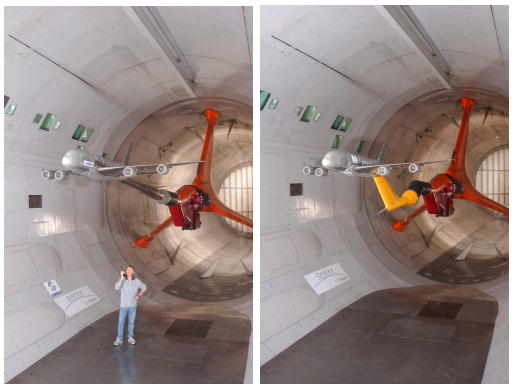

Fig. 1. View of the model and the supports.

2.2 Wind tunnel tests

This model was tested in S1MA wind tunnel in 2003, during an entry dedicated to the measurement of support effects. To serve that purpose, the model was mounted on a twin

sting rig in the test section n°3 of the S1MA wind tunnel. The twin sting rig can itself hold a dummy support carrying no load, but whose shape closely represents the real support under investigation. Measurements are then carried out with and without dummy supports, and the differences interpreted as support effects. The process to compare experiments or computational simulations with and without support will further be developed in section 3.

During the tests, the rear end of the model was cut downstream of the wing and forces on that part were measured thanks to an internal six-component balance. Forces on the front part of the model, including the wing, were not measured. The model was also equipped with about 150 static pressure taps, mainly concentrated on the rear end of the model.

2.3 Conventional support corrections

The topic of support correction has been addressed since the advent of wind tunnel testing ([14]) and was dedicated a large amount of studies since then (a sample of which can be found in [9]).

A first approach to support interference effects, quite old but still widely used, relies on potential flow theory. It will be shown later that it still can deliver some valuable results at a very cheap cost and is therefore briefly described below.

Under the assumption that the flow in the tunnel is irrotational ou

tside the boundary layers and wakes, it can be described by a velocity potential $U_0 x + \varphi$. Assuming now that the velocities $\partial_x\varphi$, $\partial_y\varphi$ and $\partial_z\varphi$ are small with regard to U_0, one comes to the well-known linearized potential equation:

$$\left(1-M_0^2\right)\partial_x^2\varphi+\partial_y^2\varphi+\partial_z^2\varphi=0\,, \qquad (1)$$

with boundary conditions at solid walls linearized as well.

Unfortunately, this last assumption is less and less valid as the upstream Mach number M_0 approaches 1 and as typical transonic phenomena occurs on the model, with large fluid accelerations up to supersonic regime.

This equation and the corresponding boundary conditions can be solved through a distribution of singularities on the model and support. The intensity of each singularity is based on the cross section areas, the lift and the drag.

Once the proper singularities have been set up, the linearity of equation 1 allows to break down the potential φ into a field φ_m generated by the model and a field φ_s generated by the support. Hence $\nabla\varphi_s = (u_s, v_s, w_s)$ is the field of velocity distortion generated by the support.

Once the velocity field $\nabla\varphi_s$ is known, one can easily determine a field of Mach number distortion:

$$\delta M = M_0\left(1+\frac{\gamma-1}{2}M_0^2\right)\frac{u_s}{U_0}\,, \qquad (2)$$

and a field of angle of attack (AoA) distortion or upwash:

$$\delta\alpha=\frac{w_s}{U_0}\,. \qquad (3)$$

These fields are then averaged in space over areas of aerodynamic significance. This averaging operation lives room for arbitrariness and the following definitions should be regarded merely as conventional, as will be investigated later on.

The Mach number correction ΔM is taken as the value of δM at ¼ of mean aerodynamic chord. The AoA correction is computed from a slightly more elaborated process: it is chord-averaged along the wing span, at ¾ of local chord, this correction enabling the lift correction to be zero (theory of Pistolesi).

A program called DXV877 has been in used in Onera wind tunnels for two decades to perform the above described computations. Results from this software will be referred as “DXV”.

This first approach based on potential equation obviously suffers from some shortcomings:

- the range of validity of the linearized potential equation in terms of Mach number is difficult to appreciate;
- results are applicable to correct upstream Mach number and AoA, but not the model forces.

In practice, such an approach must always be complemented by experimental twin sting measurement in order to derive a full set of support corrections. In order to investigate the limit of validity of the singularity approach, and to provided more complete correction data, more elaborate simulations of the flow field around the model and support were undertaken and are described in the next section.

2.4 Numerical simulations

Solving the steady Reynolds-Averaged Navier-Stokes (RANS) equations for complex configuration has now become routine task in research and industry. It has occasionally been used to model support effects [1][3][5][6] and is regarded as a promising method to supplement classical approaches, either from potential flow theory or from twin sting testing.

In this section are described the numerical models and software used to solve the steady RANS equations for the addressed configurations. For all computations, the Mach number and AoA were in the range 0.85 to 0.89 and 0° to 3°, while the Reynolds number based on mean aerodynamic chord (MAC) was 4.8 10^6, comparable to experimental.

2.4.1 elsA solver and computations

The *elsA* software is a flow solver developed by Onera and associated partners for aerospace applications [2]. It deals with external and internal aerodynamics. The solver is based on a cell-centered finite volume technique for multiblock structured grids.

For this study, the two-equation turbulence model k–ω of Menter was selected. The boundary layer was modelled on the aircraft and on the support surface thanks to proper boundary conditions and mesh refinement. No reflection boundary condition was used on the far-field surfaces. Mean flow equations were solved thanks to a Jameson second order spatial scheme, using coefficients of artificial dissipation of 0.25 for second order and 0.016 for fourth order, and Martinelli correction with an exponent of 0.3. Iterative method for time marching was a first order backward Euler scheme, associated with implicit scalar LU-SSOR solving with 4 relaxation cycles. To improve convergence, local timestep and a 2-level multigrid cycle were used.

The mesh of the configuration takes advantage of the Chimera capabilities of the solver. A mesh of the model itself, comprising about 11 million cells, is realised first. The mesh of the support, comprising about 0.5 million cells, is then built independently and overset with the model mesh as depicted in Fig.2. The individual grids overlap, and once combined cover the entire computational domain. This chimera technique allows computational grids to be generated quickly and easily.

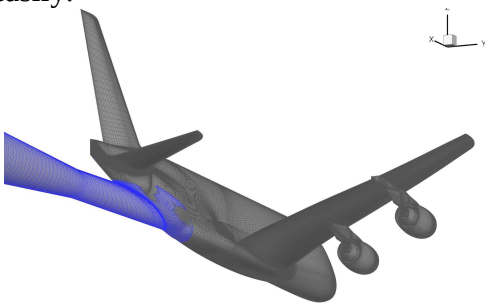

Fig. 2. Surface structured mesh of the configuration

Provided a suitable mesh of the model is already available, which is generally the case for aircraft under development being tested in wind tunnels, the meshing effort to study support effects is greatly reduced.

2.4.2 Tau solver and computations

The Tau software is a flow solver developed at DLR to simulate the external flows in aerospace applications. A finite volume, cell-vertex approach is used on hybrid unstructured grids. This software was only used for comparison purposes.

Computations presented hereafter used the Spallart-Almaras turbulent model. The boundary layer on the model and support is accurately captured thanks to 29 layers of prismatic cells. Proper mesh convergence is ensured thanks to progressive refinement of the grid during the computation.

Contrary to elsA computations, one mesh is built for the configuration without support, and another mesh is generated for the configuration with support. The meshes comprised about 12 million points (see Fig. 3).

Mean flow equations were solved thanks to a Jameson second order spatial scheme. Iterative method for time marching was a first order backward Euler scheme, associated with implicit scalar LU-SGS solving with 4 relaxation cycles. To improve convergence, a 3-level multigrid cycle was used.

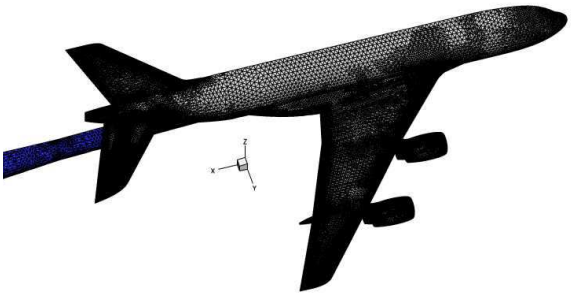

Fig. 3. Surface unstructured mesh of the configuration

3 Principles of support corrections

Determining support interference effect, either by experimental or computational means, obviously implies comparing the flow field around the configuration with support to the flow field around the configuration without support. This comparison is less trivial than it appears at first sight and is explained in this section.

3.1 The need for Mach number and AoA corrections

Let us consider in the Fig. 4 the situation labeled *a)*, which is our reference flow-field without support. The Mach number M_{ref} and AoA α_{ref} of the model can be easily defined by looking at flow conditions far upstream from the model. Pressure and force coefficients are defined in a usual way. Let us now consider the situation labeled *b)*, in which the support was introduced. The upstream Mach number and AoA are now M' and α'. One first effect of the support is to introduce a change ΔM in average Mach number and a change $\Delta\alpha$ in AoA over the model compared to upstream flow condition. For instance, in the present study the support slows the flow down at model location, so that ΔM is negative. This is standard case for support interference [1][3].

Having this in mind, two different approaches can be followed to derive support interference effects [9]:

- let M' be equal to M_{ref} and α' to α, simulate and compare situation *b)* to *a)* in order to derive a support effect under the form of force and pressure increments only;
- or let $M'+\Delta M$ be equal to M_{ref} and $\alpha'+\Delta\alpha$ to α_{ref}, then simulate and compare situation *b)* to *a)* to derive force and pressure increment. In this case, the support effect is composed of increments of Mach number, AoA, forces and pressure.

In the present study, we adopt the second formulation, arguing that it is close to common wind tunnel definition of the Mach number and AoA which generally includes corrections to cancel mean distortions originating from the the support. In fact, ΔM and $\Delta\alpha$ account for mean flow distortion at the model location. If the distortion was homogeneous in space, these corrections would be sufficient to exactly retrieve the reference flow field and forces. Therefore they can be seen as first order correction. The differences in pressure or forces remaining after Mach and AoA corrections account for the inhomogeneity of the distortion generated by the support and can be called second order corrections.

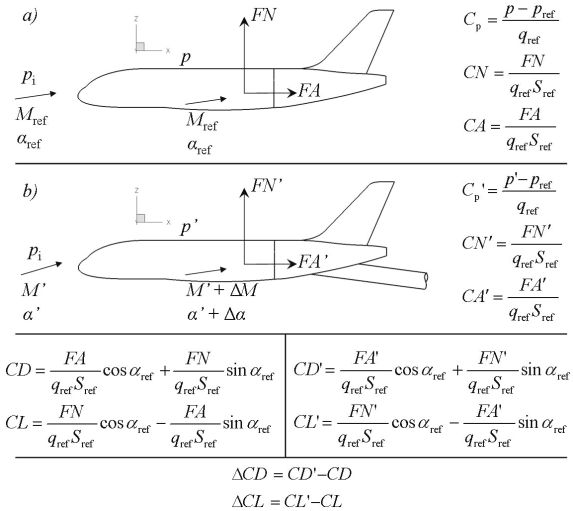

Fig. 4. Nomenclature

One last thing to mention is the use of reference Mach number and AoA to compute force and pressure coefficients, for both situation *a)* and *b)*.

3.2 Assessment of Mach number and AoA corrections

It was stated in previous section that ΔM and $\Delta\alpha$ account for mean flow distortion at the model location. In order to implement this definition in practical experiments or computations, one needs to address the notion of 'distortion', 'mean' and 'model location'. Once again, any definition implies a part of arbitrariness, justified by physical or practical considerations.

From the standpoint of linearized potential theory, the idea of distortion is straightforward: it is the velocity generated by singularities associated to the support. The averaging process to come up with a mean value was presented in section 2.3.

To deal with numerical simulations, and following [1], let us introduce the following criterion J as the RMS of pressure coefficient distortion on the wing:

$$J = \sqrt{\int_{\text{wing}} \left(C_p{}' - C_p \right)^2 \frac{dS}{S_{\text{wing}}}} . \qquad (4)$$

Because C_p' depends on the choice of ΔM and $\Delta\alpha$, J is also a function of ΔM and $\Delta\alpha$. This criterion is expected to be a measurement of the fidelity of the flow with support to the flow without support. Seeking for a minimum of distortion, let us define:

$$(\Delta M, \Delta\alpha) = \arg\min(J) . \qquad (5)$$

With this definition, first order corrections (ΔM, $\Delta\alpha$) are found after a minimization process.

4 Results

Once a definition for the Mach number and AoA correction is established, a sting effect (on both straight and Z sting) can be calculated and compared to experimental results. It is reminded that the sting interference effect is defined as the difference in forces between 'sting off' and 'sting on' configurations.

4.1 Straight sting

4.1.1 Mach number and AoA corrections

In order to identify the corrections defined by Eq. 5, the (ΔM, $\Delta\alpha$) space is explored until the optimum is identified with sufficient accuracy. From the sampled values, the J-criterion was interpolated by Kriging method to produce the Fig. 5 (TAU calculation, no research for elsA computations). A qualitative analysis of the obtained database reveals that J is mainly a sensor for the shock wave position, which is mainly driven by the Mach number in the flow condition under study and for this wing design. It explains why the J-criterion is much more sensitive to this variable. Like on most transonic airfoil at design point, the shock wave moves downstream when the Mach number or AoA increases.

The J-criterion leads to an optimum (ΔM=*-0.0025*, $\Delta\alpha$=*0*) against (ΔM=*-0.0018*, $\Delta\alpha$=*0.007*) for the ONERA-DXV method. The two methods give slightly the same results, considering the usual order of magnitude of accuracy in wind tunnel (1.10^{-3} in Mach number and 1.10^{-2} in AoA).

4.1.2 Support effect on flow-field

As no research for J-criterion has been made with elsA computations, the results are presented with ONERA-DXV upstream flow corrections.

Flow distortion generated by the straight sting can be observed in Fig. 6 that displays pressure coefficient distortion on the model skin (obtained by elsA and TAU code). Experimental results obtained by twin-sting tests are added to the comparisons. One can observe on the figure that the agreement between CFD and experimental results is rather good. The agreement is less satisfactory on the rear end of the fuselage, especially with TAU computations which predict a slowdown of the flow on that area. This can be easily seen on Fig. 7 which presents pressure distortion on the fuselage at different positions.

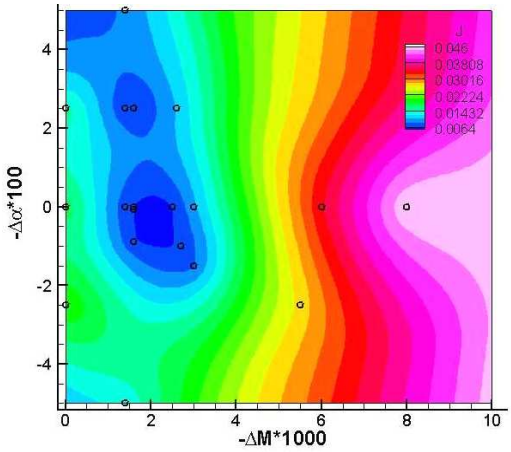

Fig. 5. RMS of wing pressure distribution with straight sting for various ΔM and Δα (TAU computations). Circles indicate sampled point. Reference flow condition is Mach 0.85, AoA 2° corresponding to 0.502 lift coefficient.

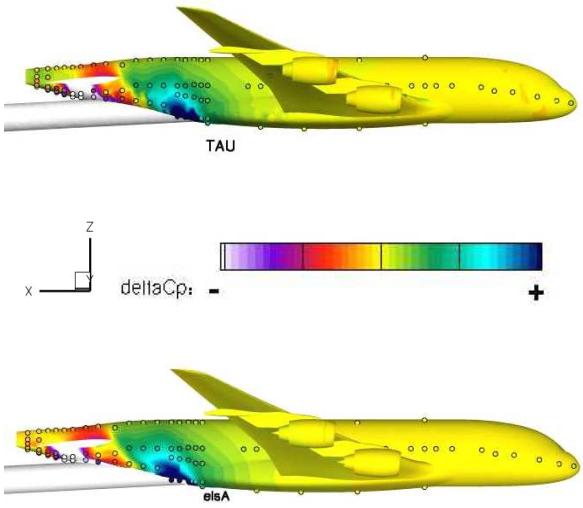

Fig. 6. Distorsion of pressure coefficient on model skin due to straight sting at M_{ref}=0.85 and α_{ref}=2° with DXV corrections on Mach and AoA. Circles indicate pressure taps colored by experimental support effect.

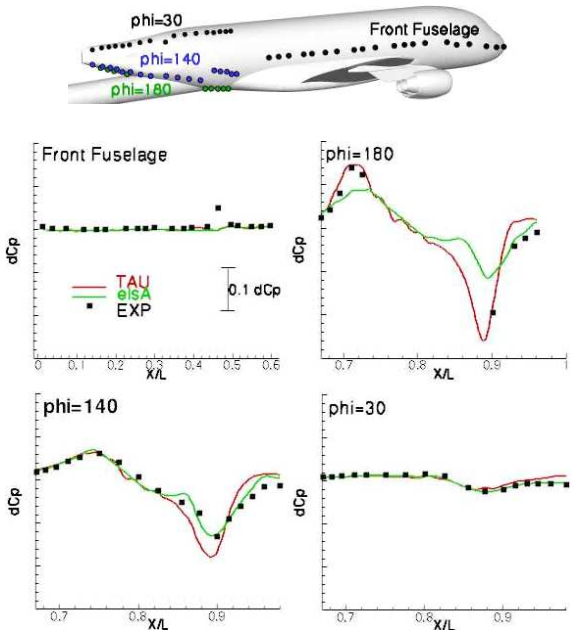

Fig. 7. Pressure increment due to straight sting on the fuselage as computed and measured during twin sting tests.

Simulations show that the very rear end of the fuselage undergoes strong thickening of the boundary layer, eventually leading to local flow separation as can be seen in Fig. 8 and Fig. 9. When the support is added to the model, an additional separation is predicted by *elsA* simulation on the top side of the support-fuselage intersection. The separated region predicted by TAU computation is much smaller than elsA prediction. This automatically leads to difference in pressure distortion.

These phenomena were shown to be very sensitive to the turbulence model (for elsA computations).

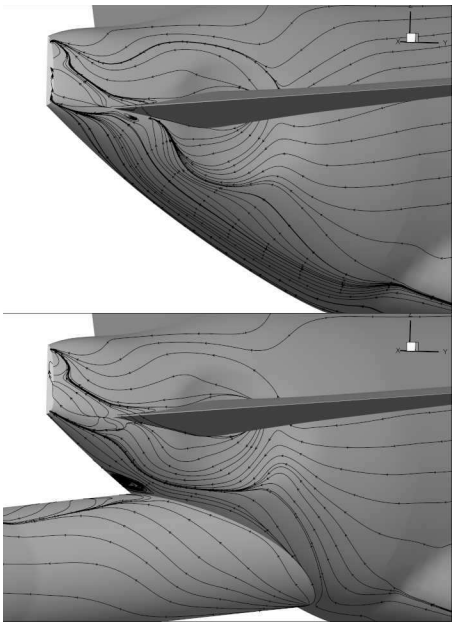

Fig. 8. Pressure coefficient and skin friction lines on the rear end of the model without support (top) and with support (bottom) – *elsA* computations.

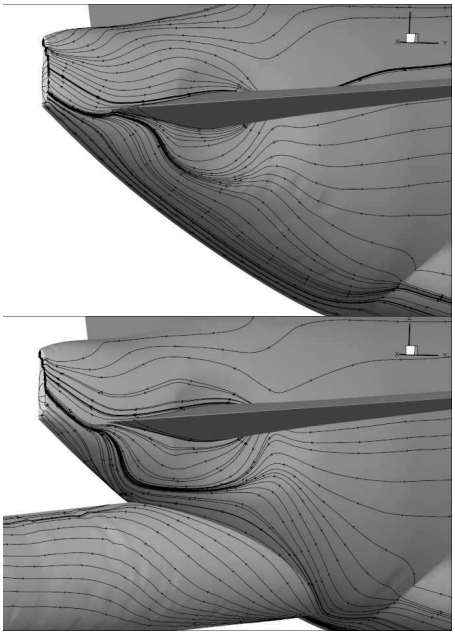

Fig. 9. Pressure coefficient and skin friction lines on the rear end of the model without support (top) and with support (bottom) – *TAU* computations.

Increments of HTP pressure due to straight sting are presented Fig. 10. Pressure increment predicted by elsA and TAU are not in very good agreement for the first section. Although, elsA results are in rather good agreement with experimental results. The sting induces a strong flow slowdown on the bottom side of the HTP near the fuselage. This slowdown is highly sensitive to the flow behavior at support-fuselage intersection. These discrepancies induce pitching moment differences on the HTP as discussed in section 4.1.3.

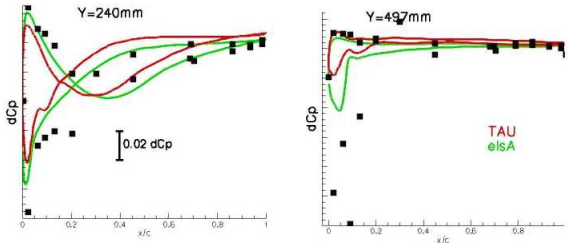

Fig. 10. Pressure increment due to straight sting on the HTP as computed and measured during twin sting tests.

4.1.3 Support effect on forces

Experimental data available for the rear part (rear body+HTP+VTP) are provided thanks to the balance integrated in the fuselage. The balance reading is corrected (among other phenomena) for split plane pressure. This correction is very large compared to the quantity measured and is the major source of inaccuracy. Indeed, uncertainty associated with the cavity pressure measurement translates into $\pm 1.10^{-4}$ uncertainty for rear body drag.

Comparison of sting effect on forces derived by CFD simulations with the experimental sting effect is carried out Fig. 11.

Sting effect on drag is different of about 2.5 drag point on the HTP between TAU and elsA computations. Experimental results predict a drag increment of about 3.10^{-4} (cruise lift) on the total rear part whereas TAU and elsA computations predict a drag increment of -3.10^{-4} and 0 respectively.

The far-field effect on the front part is well predicted by computations, DXV predictions come from the classical Archimedean formula.

The opposite sign of ΔCD for the front and rear body explains why the total experimental drag effect is null.

The effect of supports on lift coefficient is small (less than 0.002). No dependency with AoA is observed in experiment and is accurately predicted by both computations. TAU computations still predict a larger effect than elsA on the HTP.

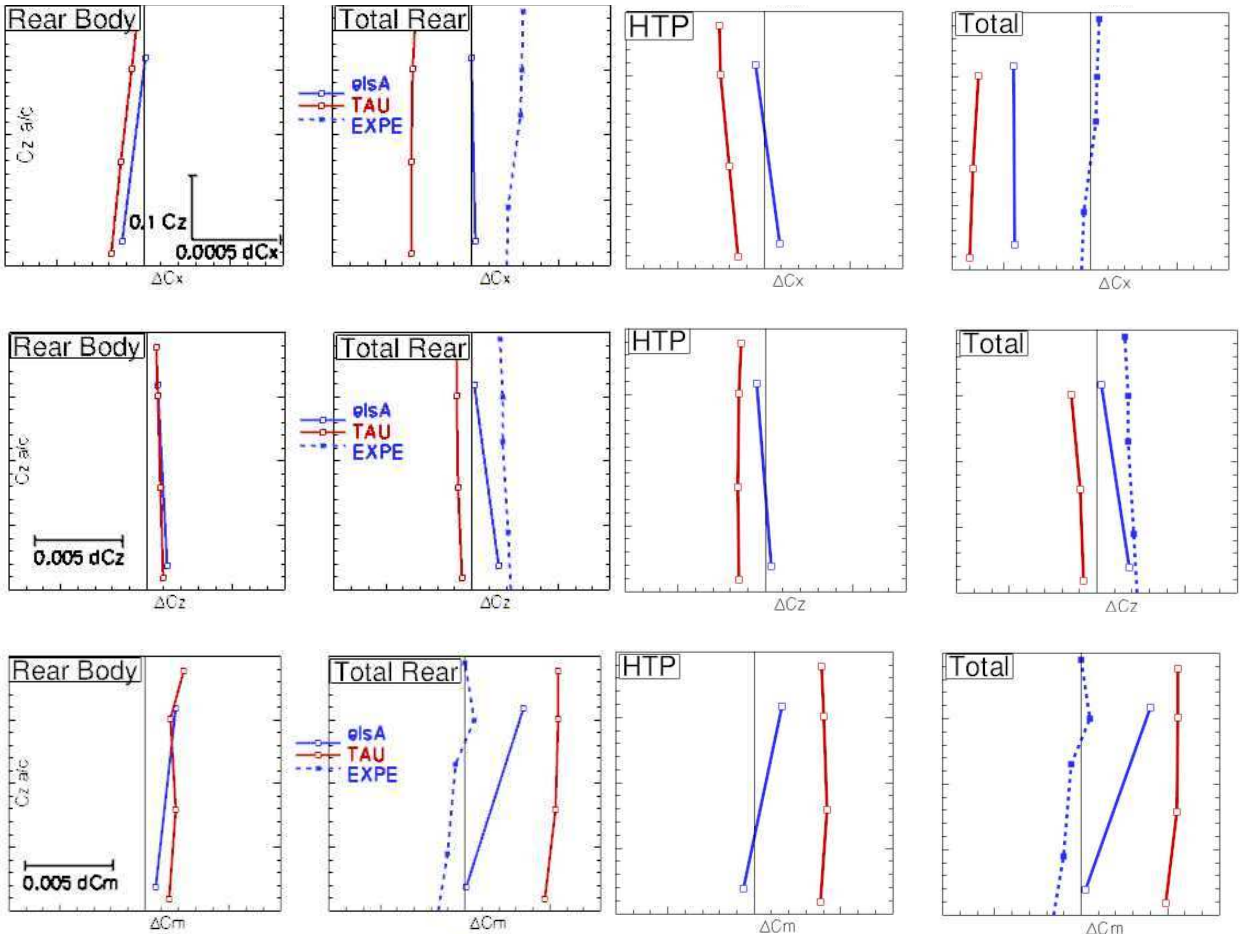

Fig. 11. Force increments due to straight sting on the rear part and on the complete model as computed by CFD and measured.

Concerning pitching moment, the effect is rather important and different between computations and experimental results for HTP. TAU computations predict an effect of 0.005 with no dependency with AoA, elsA results range between 0 and 0.004 and experimental results are constant near zero.
The disagreement between TAU and elsA on the HTP comes from the difference in flow topology between the two computations.
Although, the disagreement with experimental results have not been explained.
These phenomena are expected to be sensitive to local geometrical detail, namely the gap between the support and the fuselage. Modeling this gap is expected to improve the accuracy of the simulations and is part of ongoing work. In fact, the cavity problem is of high importance for straight stings, which cavity has a large surface facing the drag axis.

4.2 Z sting

No elsA computations have been made yet for the Z-sting effect.

4.2.1 Mach number and AoA corrections

The same methodology as for straight sting corrections has been employed. The J-criterion leads to an optimum $\Delta M=-0.0032$, $\Delta\alpha=0{,}015$) against ($\Delta M=-0.0027$, $\Delta\alpha=0{,}029$) for the ONERA-DXV method. The two methods still give slightly the same results, considering the usual order of magnitude of accuracy in wind tunnel.

4.2.2 Support effect on flow-field

Flow distortion generated by the Z sting can be observed in Fig. 12 that displays pressure coefficient distortion on the model skin.
Experimental results obtained by twin-sting tests are added to the comparisons. One can

observe on the figure that the agreement between CFD and experimental results is rather good, even on the rear end of the fuselage where discrepancies existed with straight sting effect. This can be easily seen on Fig. 13 which presents pressure distortion on the fuselage at different positions.

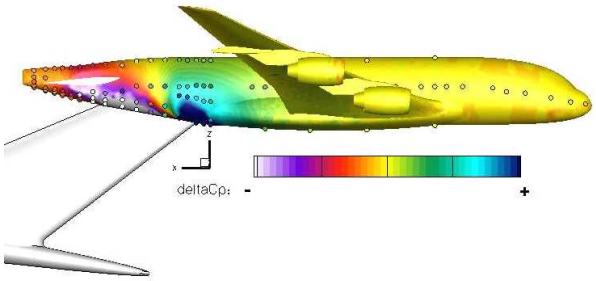

Fig. 12. Distorsion of pressure coefficient on model skin due to Z sting at M_{ref}=0.85 and α_{ref}=2° with DXV corrections on Mach and AoA. Circles indicate pressure taps colored by experimental support effect.

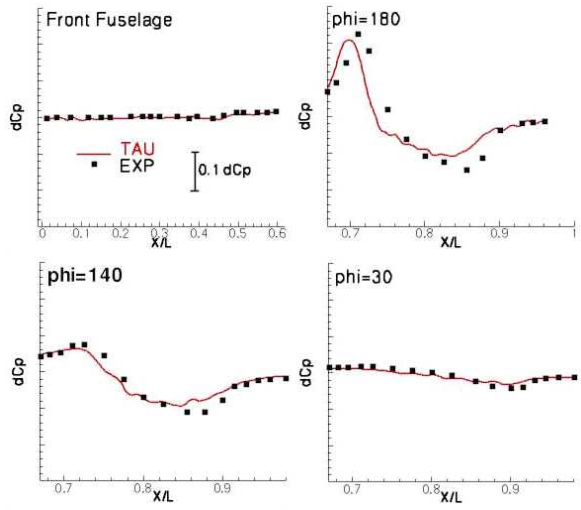

Fig. 13. Pressure increment due to Z sting on the fuselage as computed and measured during twin sting tests.

Increments of HTP pressure due to Z sting are presented Fig. 14. Pressure increments predicted by TAU are in rather good agreement with experimental results.

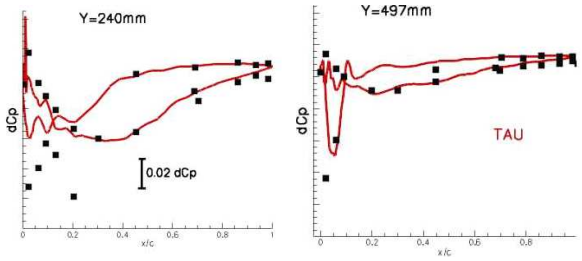

Fig. 14. Pressure increment due to Z sting on the HTP as computed and measured during twin sting tests.

4.2.3 Support effect on forces

Comparison of Z-sting effect on forces derived by CFD simulations with the experimental sting effect is carried out Fig. 15.
Sting effect on drag is very well predicted by computations. The agreement is within $1.5.10^{-4}$ all over the polar range.
The far-field effect on the front part is well predicted by computations, DXV predictions come from the classical Archimedean formula.
The effect of supports on lift coefficient is small (less than 0.002). No dependency with AoA is observed in experiment and is accurately predicted by computations.
Concerning pitching moment, the effect is rather important and still different between computations and experimental results for HTP. TAU computations predict an effect of 0.007 with no dependency with AoA, experimental results are constant at 0.002.
The disagreement with experimental results has not been explained. But the disagreement between numerical and experimental results on pitching moment is of 5.10^{-3} for both stings.

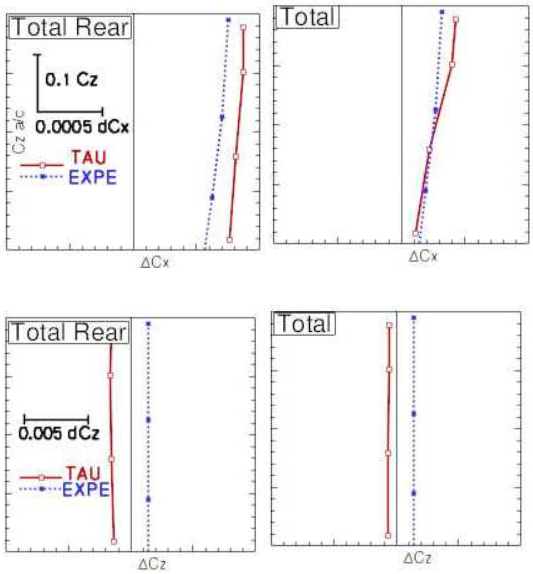

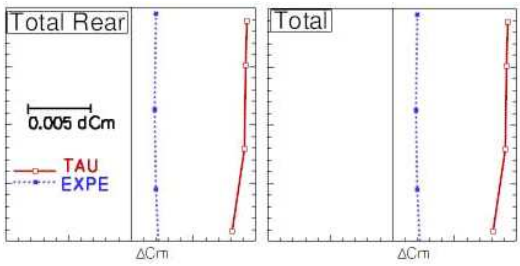

Fig. 15. Force increments due to straight sting on the rear part and on the complete model as computed by CFD and measured.

5 Conclusions and perspectives

The interference effects of two different stings support for S1MA wind tunnel were assessed by means of CFD computations. Special attention was paid to the proper deviation of corrections of the incoming flow conditions in terms of Mach number and angle of attack.

The computed upstream corrections were very close to the DXV calculations. This could allow us to avoid the full exploration of the (ΔM, $\Delta\alpha$) space which is time consuming.

The calculated sting effects were compared to twin sting tests. Comparison on the straight sting showed it hard to predict a correct drag effect as we might have a separated region at fuselage-sting intersection. That is why the next step is to take into account the gap between the fuselage and the sting.

The Z sting drag effect was although well predicted within $1.5.10^{-4}$. Both sting effects on lift are very small and well predicted. We although have a constant difference of 5.10^{-3} in pitching moment between computations and experiments on both stings. This difference has not yet been explained.

References

[1] Mouton S. Numerical Investigations of Model Support Interference in a Transonic Wind Tunnel. *44ème Colloque d'aérodynamique appliquée AAAF*, Nantes, March 23-25, 2009.

[2] Cambier L, Veuillot J-P. Status of the *elsA* CFD Software for Flow Simulation and Multidisciplinary Applications. AIAA 2008-664, Reno, January 7-10, 2008.

[3] Mouton S. Numerical Investigations of Model Support Interference in Subsonic and Transonic Wind Tunnels. 8th ONERA-DLR Symposium ODAS 2007, Göttingen, October 17-19, 2007

[4] Schamborn D, Gerhold T, Heinrich R. The DLR Tau-Code: Recent Applications in Research and Industry. *European Conference on Computational Fluid Dynamics*, 2006.

[5] Maina M, Corby N, Crocker EL, Hammond PJ, Wong PWC, A Feasability Study on Designing Model Support Systems for a Blended Wing Body Configuration in a Transonic Wind Tunnel. *The Aeronautical Journal*, January 2006

[6] Bush RH, Jasper DW, Parker SL, Romer WW, Willhite PG. Computational and Experimental Investigation of F/A-18E Sting Support and Afterbody Distorsion Effects. *Journal of Aircraft*, Vol. 33, No. 2, March-April 1996.

[7] Lyonnet M, Piat J-F, Roux B, Model Support Interference Assessment Using a Metric Rear Fuselage and a Twin-Sting at ONERA S2MA Wind Tunnel. *International Conference on Experimental Fluid Mechanics*, Turin, July 4-8, 1994.

[8] Lynch FT, Crites RC, Spaid FW. The Crucial Role of Wall Interference, Support Interference, and Flow Field Measurements in the Development of Advanced Aircraft Configurations. AGARD CP-535, 1993.

[9] *Wall Interference, Support Interference and Flow Field Measurements.* AGARD CP-535, 1993.

[10] Elsenaar A, Han SOTH, *A Break-Down of Sting Interference Effects.* NLR TP 91220 U, May 1991.

[11] Vaucheret X. Recent Calculation Progress on Wall Interferences in Industrial Wind Tunnels. *La Recherche Aérospatiale*, No. 3, pp 45-47, 1988.

[12] Loving DL, Luoma AA. *Sting-Support Interference on Longitudinal Aerodynamic Characteristics of Cargo-Type Airplane Model at Mach 0.70 to 0.84.* NASA Technical Note TN D-4021, July 1967.

[13] Love ES. *A Summary of Information on Support Interference Assessment at Transonic and Supersonic Speeds*. NACA RM L53K12, 1954.

[14] Pankhurst RC, Holder D. *Wind-Tunnel Technique.* Sir Isaac Pitman & Sons, 1952.

Copyright Statement